Optics Letters

Smartphone-based bimodal device (SBBD) for oral precancer diagnosis and biopsy guidance in clinical settings

Nemichand,[1] Shivam Shukla,[2] Bhaswati Singha Deo,[2] Amar Nath Sah,[3] Subrata Mishra,[4] Rachna Rath,[5] and Asima Pradhan[1,2,3,4,*]

[1]Department of Physics, Indian Institute of Technology Kanpur, Kanpur 208016, India
[2]Center for Lasers and Photonics, Indian Institute of Technology Kanpur, Kanpur 208016, India
[3]Siksha 'O' Anusandhan, Bhubaneswar 751030, India
[4]PhotoSpIMeDx Pvt. Ltd., SIIC, IIT Kanpur & SOA, Bhubaneswar, India
[5]Department of Oral Pathology and Microbiology, SCB Government Dental College and Hospital, Cuttack 753007, India
*asima@iitk.ac.in

Received 9 January 2025; revised 10 February 2025; accepted 12 February 2025; posted 12 February 2025; published 10 March 2025

We present a smartphone-based bimodal device (SBBD) combining fluorescence imaging and spectroscopy for a noninvasive, portable, cost-effective, and real-time diagnosis of oral precancer. The device employs a 405 nm laser excitation to capture native fluorescence from intrinsic biomarkers, including flavin adenine dinucleotide (FAD) and porphyrin, across 136 subjects representing normal, OPMD, and OSCC. The fluorescence imaging module identifies regions of interest (ROI) based on the red-to-green band ratio ($\frac{\text{porphyrin}}{\text{FAD}}$), while the spectroscopy module confirms findings through multiple point measurements. A 2D convolutional neural network (CNN) classifies normal tissues, oral potentially malignant disorders (OPMD), and oral squamous cell carcinoma (OSCC) with 97.04% accuracy, 96.13% sensitivity, and 97.73% specificity. Fluorescence spectroscopy, enhanced by an artificial neural network (ANN), achieves 97.44% accuracy, 95.24% sensitivity, and 97.44% specificity. This bimodal approach effectively addresses the diagnostic gap that occurs when either spectroscopy or imaging is used independently for oral cancer detection and biopsy guidance. © 2025 Optica Publishing Group. All rights, including for text and data mining (TDM), Artificial Intelligence (AI) training, and similar technologies, are reserved.

https://doi.org/10.1364/OL.555254

Globally, oral cancer ranked 16th, with approximately 377,000 new cases and 177,000 deaths reported in 2020, while in India, it is ranked 2nd, with 77,000 new cases annually [1,2]. High mortality, with a 5-year survival rate of less than 40%, is primarily due to late diagnosis and the lack of portable, noninvasive diagnostic tools [3]. Fluorescence imaging and spectroscopy provide rapid, noninvasive, and highly sensitive alternatives for early cancer detection [4–7]. However, many commercially available devices for oral cancer detection, such as VELscope, OralID, and VisiLite, rely solely on autofluorescence imaging, limiting their diagnostic accuracy [8,9]. Table S1 (see Supplement 1) provides the diagnostic methods and clinical performance statistics for these commercial devices.

Fluorescence spectroscopy effectively detects biochemical changes in tissues, with alterations in endogenous fluorophores serving as biomarkers for oral cancer [10]. Morphological changes can be detected through fluorescence imaging, which also plays a crucial role in guiding both spectroscopy and biopsy [11]. Combining spectroscopy with imaging offers the potential for more accurate diagnosis, and recent studies have shown promising results in oral and aorta cancer diagnostics [12,13]. However, using imaging as a guide for spectroscopy and biopsy remains unexplored.

In this Letter, we introduce a smartphone-based bimodal device (SBBD) that integrates fluorescence imaging and spectroscopy for noninvasive, real-time diagnosis of oral precancer. Smartphones offer an ideal platform for portable, low-cost devices, leveraging their wireless capabilities, advanced sensors, and computing power for diverse applications, including fluorescence imaging and spectroscopy [14–16]. Our device utilizes the smartphone as both a detector and power source, providing a compact and accessible solution for fluorescence detection. The combination of imaging for lesion visualization and spectroscopy for molecular analysis significantly improves diagnostic accuracy. Machine learning algorithms classify clinical results, making the device well-suited for resource-limited settings. Previous studies by our group indicate that the relative concentrations of porphyrin (red band) and FAD (green band) vary with disease progression, suggesting that the R/G ratio could be an effective parameter for identifying regions of interest (ROI) [6,7]. Imaging modality effectively distinguishes abnormal regions from surrounding healthy tissues using the R/G ratio, significantly improving tumor visualization. The SBBD, validated through *in vivo* testing, demonstrates strong potential for scalable, portable cancer diagnostics.

We developed a smartphone-based bimodal device (SBBD)

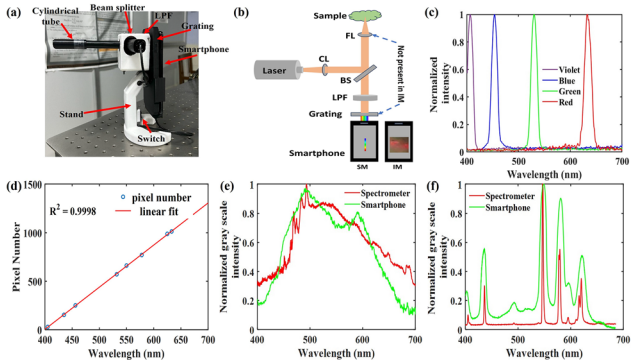

Fig. 1. (a) Smartphone-based bimodal device (SBBD). (b) SBBD optical assembly integrating the imaging (IM) and spectroscopy (SM) modules, with switchable operation (BS, beam splitter; LPF, long-pass filter; CL, collimating lens; FL, focusing lens). (c) Emission spectra of a continuous light source captured by the SBBD in violet, blue, green, and red bands of the visible spectrum. (d) Calibration curve for the SM using a continuous light source. (e) Xenon lamp spectra recorded by both the commercial and smartphone-based spectrometers. (f) Comparison of mercury lamp spectra recorded by a commercial spectrometer and the smartphone-based spectrometer.

[17] for oral precancer diagnosis, integrating fluorescence imaging and spectroscopy [Fig. 1(a)]. The system has two modules: the imaging module (IM) and spectroscopy module (SM). A 405 nm laser (Adlabs Instruments, New Delhi) excites the sample, and the fluorescence is captured by a Redmi K20 smartphone camera through a 450 nm filter (OD 4.0 LPF, Edmund Optics) [Fig. 1(b)]. The SM includes a focusing lens (LA1576, Thorlabs, 12 mm focal length) and a transmission grating (GT13-12, Thorlabs, 1200 grooves/mm) aligned parallel to the camera and at a 45° angle with respect to the optical assembly, for generating spectral images. The device switches easily between IM and SM, ensuring that both spectra and images are captured from the same region of interest. The device features a PLA cradle and disposable cap for medical use, with a PETG casing for durability. The device's imaging module (IM) captures fluorescence intensity through a 450 nm long-pass filter, storing images in the RGB format. The spectroscopy module (SM) directs fluorescence signals onto a transmission grating, dispersing light onto the mobile camera sensor to record emitted fluorescence in the RAW format. Calibration was done using a visible light source (400–700 nm), with emission peaks captured in violet, blue, green, and red bands [Fig. 1(c)], showing a linear correlation between pixel position and wavelength [Fig. 1(d)]. Spectra from a xenon lamp aligned with a commercial spectrometer [Fig. 1(e)], and the system detected multiple peaks. Using a mercury lamp, the smartphone spectrometer effectively captured distinct emission lines, though it exhibited a broader FWHM (13.86 nm vs. 2.69 nm for the commercial spectrometer) at 547 nm [Fig. 1(f)]. In a phantom study, the IM module displayed green and red bands corresponding to FAD and porphyrin, respectively [Fig. 2(a)], confirming sensitivity to fluorophore concentration changes [Fig. 2(b)]. The SM captured FAD's emission peak at 525 nm with a limit of detection (LOD) of 0.005 μM evaluated using the equation $\mathrm{LOD} = 3\sigma/s$ [18] [Fig. 2(c)] and porphyrin's peaks at 630 nm and 670 nm with a LOD of 0.04 μM [Fig. 2(d)], highlighting the system's potential for oral cancer detection.

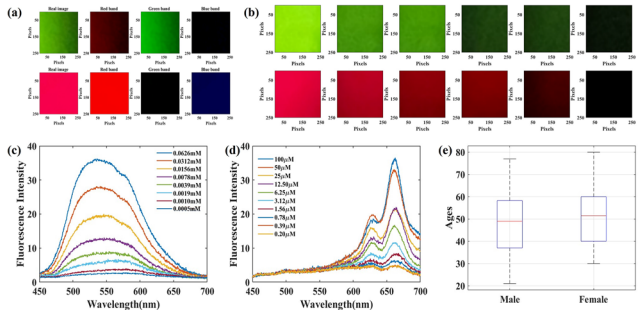

Fig. 2. (a) Fluorescence images of FAD and porphyrin liquid phantoms and the corresponding band-extracted images, captured by the SBBD's imaging module. (b) Fluorescence images of liquid FAD and porphyrin fluorophores at varying concentrations (FAD, 0.0312 mM, 0.0156 nM, 0.0078 mM, 0.0039 mM, 0.0019 mM, 0.0010 mM; porphyrin, 50 μM, 25 μM, 12.50 μM, 6.25 μM, 3.12 μM, 1.56 μM; left to right), captured by the SBBD. (c) Fluorescence spectra of liquid FAD fluorophore at varying concentrations, captured using the SBBD. (d) Fluorescence spectra of liquid porphyrin fluorophore at varying concentrations, captured using the SBBD. (e) Box plot comparing the age distribution of male and female patients involved in the study.

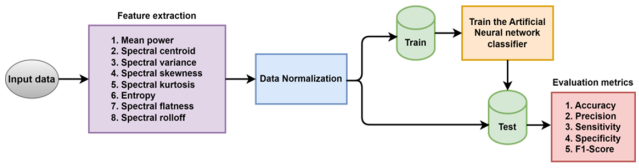

Fig. 3. Architecture of the spectral data classification.

This study used a SBBD for *in vivo* testing at SCB Dental College and Hospital, Cuttack, Odisha. It involved two groups: a control group of healthy volunteers and a study group with patients showing symptoms such as whitish or reddish patches, mixed patches, or raised growths (excluding ulcers/infections). A total of 136 individuals (136 spectra and 454 images) participated, including 37 OSCC patients, 59 with OPMDs (29 with OSMF, 25 with leukoplakia, and 5 with lichen planus), and 40 normal volunteers. Data were collected from the buccal mucosa, dorsal surface of the tongue, soft palate, and lateral border of the tongue. The median age for males was 49 years (IQR, 38–59; range, 21–77), and for females, 52 years (IQR, 40–60; range, 30–80) [Fig. 2 (e)].

The proposed classification framework for the spectral data is shown in Fig. 3. The proposed methodology starts with the acquisition of input data, followed by an important feature extraction phase where several spectral features are calculated to capture the characteristics of the signal. These features include mean power, spectral centroid, spectral variance, spectral skewness, spectral kurtosis, entropy, spectral flatness, and spectral roll-off. After feature extraction, these values are normalized, and the normalized data is used to train an artificial neural network (ANN) classifier. The classification network used in the study is an ANN structured with three hidden layers and an output layer tailored for multi-class classification as shown in Table S2 (see Supplement 1).

The proposed classification framework for the imaging data is shown in Fig. 4. Each image is resized to a standard target size of 224 × 224 pixels, which is a commonly used input size for deep

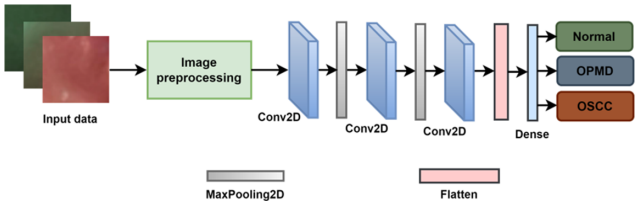

Fig. 4. Block diagram of the proposed 2D CNN classifier.

learning models, such as convolutional neural networks (CNNs). After resizing, the pixel values are normalized by scaling them to a range of 0–1 by dividing by 255, ensuring consistent pixel value representation across the dataset. In addition to normalization, data augmentation techniques are employed using the ImageDataGenerator class. These augmentation techniques include random rotations up to 20°, horizontal and vertical shifts up to 20%, and horizontal flipping. These transformations increase the diversity of the training data, helping to prevent overfitting and enhancing the model's ability to generalize to unseen data. The CNN model used for classification is a sequential architecture that consists of several layers, each designed to progressively extract and learn features from the input images as shown in Table S3 (see Supplement 1).

The fluorescence spectra from SBBD [Fig. 5(a)] show a 500 nm peak (FAD) in normal volunteers, with OSCC patients exhibiting peaks at 500 nm (FAD) and 635 nm (porphyrin). In OPMD, the 500 nm peak dominates, while in OSCC, both peaks have similar intensity, indicating a decline in FAD fluorescence and an increase in porphyrin with disease progression, consistent with previous studies [6]. A characteristic dip at 560 nm in the spectrum arises due to the sensor's nonlinear response. Fluorescence images [Fig. 5(b)] show the green band dominating in normal tissues, increasing the red intensity in OPMD, and a further rise in the red-to-green ratio in OSCC, reflecting higher porphyrin accumulation. This shift in fluorescence suggests potential biomarkers for detecting abnormal tissue regions.

The imaging (IM) module captures fluorescence images over a 1 cm^2 area to visualize oral tissue fluorescence. In OPMD, where abnormal regions are hard to identify with conventional methods, the R/G ratio image effectively delineates regions for biopsy and spectroscopy [Fig. S1(b) (see Supplement 1)]. This ratio improves tissue abnormality visualization compared to standard fluorescence images [Fig. S1(a) (see Supplement 1)]. By applying a threshold to the R/G ratio, abnormal areas are identified in real time, offering a clearer distinction than white-light biopsy selection, which can be uncertain. The R/G ratio also reveals a peak at abnormal sites, confirming differentiation from normal tissues [(Fig. S1(c) (see Supplement 1)]. The R/G ratio image aids in selecting biopsy sites and positioning spectroscopic measurements. Figure 5(c) shows IM module images lack clear margin distinction between normal and OSCC regions, while the R/G ratio image [Fig. 5(d)] clearly defines this boundary. Fluorescence spectra from the normal, margin, and OSCC regions [Fig. 5(e)] show FAD and porphyrin peaks for OSCC, and enhanced intensity in the 600–650 nm wavelength range, indicating the presence of OSCC cells at the margin. The R/G ratio image is key for biopsy and spectroscopic guidance. Previous studies used the mean peak ratio for malignancy, but our analysis highlights the need for larger

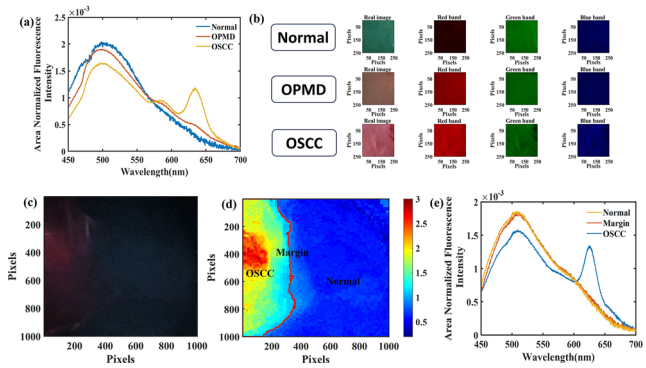

Fig. 5. (a) Representative fluorescence spectra captured by the SBBD from a normal volunteer, an individual with OPMD, and an OSCC patient. (b) Fluorescence images (250 × 250 pixels) from a normal volunteer, OPMD, and OSCC patients, captured by the SBBD. (c) Image captured by the imaging module (IM) of the SBBD from an OSCC patient (1000 × 1000 pixels). (d) Extracted R/G ratio image of the captured data, highlighting the margin line between the normal and OSCC regions. (e) Fluorescence spectrum at three positions—normal, margin, and OSCC regions—was obtained using the spectroscopic module (SM) of the SBBD.

datasets to improve reliability. To address this, machine learning was employed to classify clinical data from imaging and spectroscopy. The R/G ratio image identifies suspicious regions for spectroscopy, improving performance and biopsy accuracy, offering a significant advancement over traditional fluorescence imaging.

This section presents the results of applying the proposed framework to classify normal, OPMD, and OSCC oral cancer classes using fluorescence spectral and imaging data. The methodology for spectral data includes data acquisition, feature extraction, and normalization, followed by training an ANN model with the Adam optimizer, a learning rate of 0.001, and 1000 epochs (batch size: 10). Categorical Crossentropy was used as the loss function, with 80% data for training and 20% for testing.

The classification model's performance, evaluated through the confusion matrix [Fig. 6 (a)], shows the following macro average values for spectral data: precision 97.62%, sensitivity 95.24%, F1-score 96.20%, specificity 97.44%, and accuracy 97.44% (Table 1). The calculated parameters (precision, recall or sensitivity, F1-score, specificity, and accuracy) were derived using Eqs. S1–S5 (see Supplement 1) and are listed in Table 1. For imaging data, the model was trained for 100 epochs with a batch size of 32, achieving macro average values: precision 95.51%, sensitivity 96.13%, F1-score 95.80%, specificity 97.73%, and accuracy 97.04% [Fig. 6(b), Table 2]. Positive and negative predicted values are listed in Tables S4 and S5 (see Supplement 1).

The individual modalities of the device, imaging and spectroscopy, demonstrate strong performance when utilizing the classification algorithm. The combined use of these modalities addresses the diagnosis gaps that arise when either modality is used alone. Specifically, imaging data demonstrated superior performance in classifying OSCC cases, while spectral data excelled in classifying OPMD and normal cases with perfect sensitivity (100%) and specificity (100%). This complementary behavior ensures that the system covers cases that might be misclassified by one modality but correctly classified by the other,

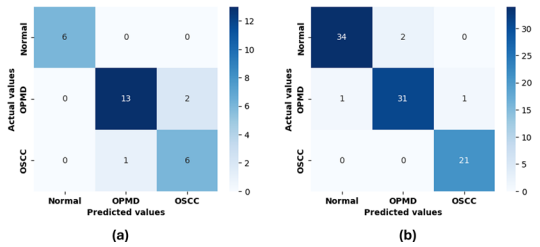

Fig. 6. Confusion matrix. (a) Spectral data. (b) Imaging data.

Table 1. Performance Evaluation Parameters of the Proposed Classification Algorithm for Spectral Data[a]

Class	Pre	Sen	F1	Spec	Acc
Normal	100	100	100	100	100
OPMD	92.86	100	96.30	92.31	96.15
OSCC	100	85.71	92.31	100	96.15
Average	97.62	95.24	96.20	97.44	97.44

[a]Pre, Precision; Sen, Sensitivity; F1, F1-Score; Spec, Specificity; Acc, Accuracy.

Table 2. Performance Evaluation Parameters of the Proposed Classification Algorithm for Imaging Data[a]

Class	Pre	Sen	F1	Spec	Acc
Normal	97.14	94.44	95.77	98.15	96.67
OPMD	93.94	93.94	93.94	96.49	95.56
OSCC	95.45	100	97.67	98.55	98.89
Average	95.51	96.13	95.80	97.73	97.04

[a]Pre, Precision; Sen, Sensitivity; F1, F1-Score; Spec, Specificity; Acc, Accuracy.

reducing the likelihood of missed diagnoses (false negatives) and incorrect diagnoses (false positives).

A smartphone-based bimodal device (SBBD) was developed to efficiently diagnose oral precancer, utilizing fluorescence signals from oral tissues. By integrating machine learning, the device demonstrates high diagnostic performance, achieving 97.04% accuracy, 96.13% sensitivity, and 97.73% specificity with fluorescence imaging and 97.44% accuracy, 95.24% sensitivity, and 97.44% specificity with spectroscopy data. This dual-modality approach minimizes diagnostic uncertainty. The red-to-green (R/G) ratio imaging technique enhanced the identification of abnormal tissues, improving diagnostic precision over conventional methods. This bimodal system advances noninvasive screening and supports precise biopsy site selection. Future efforts will focus on expanding clinical datasets and optimizing machine learning models to further improve performance and broaden clinical applicability.

Funding. This study was funded by PhotoSpIMeDx Pvt. Ltd., a company incubated at IIT Kanpur, and SOA University, Odisha.

Acknowledgment. Nemichand, Shivam Shukla, and Bhaswati Singha Deo are thankful to IIT Kanpur for the institute fellowship.

Disclosures. The authors have filed a patent application [19].

Data availability. Data underlying the results presented in this Letter are not publicly available but may be obtained from the authors upon reasonable request.

Supplemental document. See Supplement 1 for supporting content.

REFERENCES

1. P. D. Madankumar, K. Iyer, S. Soni, *et al.*, Cancer Research, Statistics, and Treatment **5**, 226 (2022).
2. H. Sung, J. Ferlay, R. L. Siegel, *et al.*, Ca-Cancer J. Clin. **71**, 209 (2021).
3. S. Abati, C. Bramati, S. Bondi, *et al.*, Int. J. Environ. Res. Public Health **17**, 9160 (2020).
4. M. Motamedi, E. van der Breggen, B. Bell, *et al.*, in *Quantum Electronics and Laser Science Conference* (Optica Publishing Group, 1999), paper LThA3.
5. P. Pande, S. Shrestha, J. Park, *et al.*, *Optics in the Life Sciences* (Optica Publishing Group, 2013), paper MT3C.2.
6. P. Kumar, S. K. Kanaujia, A. Singh, *et al.*, Lasers Med. Sci. **34**, 1243 (2019).
7. A. N. Sah, P. Kumar, and A. Pradhan, J. Fluoresc. **33**, 1375 (2023).
8. C. Wang, X. Qi, X. Zhou, *et al.*, Transl Cancer Res. **11**, 1603 (2022).
9. L. Tiwari, O. Kujan, and C. S. Farah, Oral Diseases **26**, 491 (2020).
10. M. G. Müller, T. A. Valdez, I. Georgakoudi, *et al.*, Cancer **97**, 1681 (2003).
11. I. Pavlova, M. Williams, A. El-Naggar, *et al.*, Clin. Cancer Res. **14**, 2396 (2008).
12. P. Thapa, V. Singh, S. Bhatt, *et al.*, Methods Appl. Fluoresc. **11**, 045008 (2023).
13. J. K. Barton, F. Guzman, and A. Tumlinson, J. Biomed. Opt. **9**, 618 (2004).
14. B. Hunt, A. J. Ruiz, and B. W. Pogue, J. Biomed. Opt. **26**, 040902 (2021).
15. S. Shukla, A. N. Sah, D. Hatiboruah, *et al.*, Sci. Rep. **12**, 11192 (2022).
16. H. Yu, Y. Tan, and B. T. Cunningham, Anal. Chem. **86**, 8805 (2014).
17. S. Shukla, N. Nemichand, A. N. Sah, *et al.*, *Biophotonics in Point-of-Care III, Vol. 13008* (SPIE, 2024), pp. 19–23.
18. D. Hatiboruah, T. Das, N. Chamuah, *et al.*, Measurement **154**, 107507 (2020).
19. A. Nath Sah, S. Shukla, S. Ahirwar, *et al.*, "A smartphone based oral cancer detection device using combined techniques of fluorescence spectroscopy and imaging," Indian patent application 202,211,027,171 (11 May 2022).

2025 17 209 2036-01 30 03 57 24